Accepted Manuscript

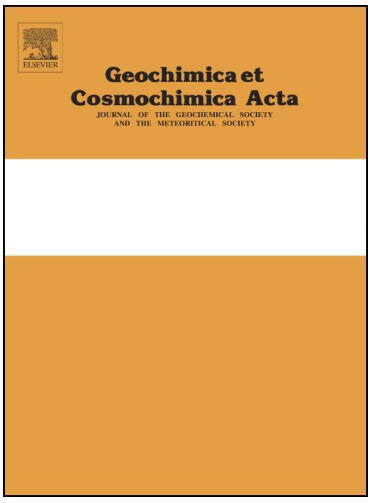

A Kinetic Pressure Effect on Calcite Dissolution in Seawater

Sijia Dong, Adam V. Subhas, Nick E. Rollins, John D. Naviaux, Jess F. Adkins, William M. Berelson

PII: S0016-7037(18)30391-0
DOI: https://doi.org/10.1016/j.gca.2018.07.015
Reference: GCA 10846

To appear in: *Geochimica et Cosmochimica Acta*

Received Date: 16 January 2018
Accepted Date: 9 July 2018

Please cite this article as: Dong, S., Subhas, A.V., Rollins, N.E., Naviaux, J.D., Adkins, J.F., Berelson, W.M., A Kinetic Pressure Effect on Calcite Dissolution in Seawater, *Geochimica et Cosmochimica Acta* (2018), doi: https://doi.org/10.1016/j.gca.2018.07.015

A Kinetic Pressure Effect on Calcite Dissolution in Seawater

Sijia Dong [a,*], Adam V. Subhas [b, c], Nick E. Rollins [a], John D. Naviaux[b], Jess F. Adkins [b], and William M. Berelson [a]

[a] *University of Southern California, Los Angeles, CA, 90089, United States*

[b] *California Institute of Technology, Pasadena, CA, 91125, United States*

[c] *Woods Hole Oceanography Institute, Woods Hole, MA, 02543, United States*

Abstract

This study provides laboratory data of calcite dissolution rate as a function of seawater undersaturation state (1- Ω) under variable pressure. ^{13}C-labeled calcite was dissolved in unlabeled seawater and the evolving δ^{13}C composition of the fluid was monitored over time to evaluate the dissolution rate. Results show that dissolution rates are enhanced by a factor of 2-4 at 700 dbar compared to dissolution at the same Ω under ambient pressure (10 dbar). This dissolution rate enhancement under pressure applies over an Ω range of 0.65 to 1 between 10 dbar and 700 dbar. Above 700 dbar (up to 2500 dbar), dissolution rates become independent of pressure. The observed enhancement is well beyond the uncertainty associated with the thermodynamic properties of calcite under pressure (partial molar volume ΔV), and thus should be interpreted as a kinetic pressure effect on calcite dissolution. Dissolution at ambient pressure and higher pressures yield non-linear dissolution kinetics, the pressure effect does not significantly change the reaction order n in $Rate = k(1- \Omega)^n$, which is shown to vary from 3.1±0.3 to 3.8±0.5 from 10 dbar to 700 dbar over Ω = 0.65 to 0.9. Furthermore, two different dissolution mechanisms are indicated by a discontinuity in the rate-undersaturation relationship, and seen at both ambient and higher pressures. The discontinuity, $\Omega_{critical}$ = 0.87±0.05 and 0.90±0.03 at 10 dbar and 1050 dbar respectively, are similar within error. The reaction order, n, at Ω>0.9 is 0.47±0.27 and 0.46±0.15 at 10 dbar and 700 dbar respectively. This $\Omega_{critical}$ is considered to be the threshold between step retreat dissolution and defect-assisted dissolution. The kinetic enhancement of dissolution rate at higher pressures is related to a decrease in the interfacial

energy barrier at dissolution sites. The impact of pressure on the calcite dissolution kinetics implies that sinking particles would dissolve at shallower depth than previously thought.

1. INTRODUCTION

The investigation of calcium carbonate dissolution in the ocean is critical in constructing global carbon budgets and understanding the ocean's role in neutralizing atmospheric CO_2 by dissolving $CaCO_3$. Most kinetics studies (Morse, 1978; Morse et al., 1979; Keir, 1980; Byrne et al., 1984; Walter and Morse, 1985; Hales and Emerson, 1997; Gehlen et al., 2005; Subhas et al., 2015) of the dissolution behavior of calcium carbonates in seawater have expressed the dependence of dissolution rate on seawater saturation state through an empirical equation of the form:

$$Rate = k(1 - \Omega)^n \quad (1)$$

where k is a rate constant, n is a positive constant known as the "order" of the reaction, Ω is the saturation state defined as the ion concentration product over the stoichiometric solubility product (K^*_{sp}):

$$\Omega = \frac{[Ca^{2+}][CO_3{}^{2-}]}{K^*_{sp}} \quad (2)$$

Ω varies either by changing the numerator – ion concentrations (water chemistry), or by changing the denominator – K^*_{sp}. In deep oceanic waters, which are undersaturated with respect to calcite, salinity varies only slightly (34 to 36), the water masses are nearly isothermal (3±2°C) and pressure is the most important influence on K^*_{sp}. At 2°C and a pressure corresponding to a depth of about 6500 m, K^*_{sp} is about 3.7 times greater than at atmospheric pressure (Ingle, 1975). Another factor that decreases Ω in the deep ocean is that respiration of sinking organic matter releases CO_2, decreases pH and [CO_3^{2-}], and thus Ω. The relative importance of these two factors (pressure and microbial respiration of organic matter) in modulating Ω was investigated in a North Pacific Ocean Section (Fig. 1). Ω_{real} is the actual Ω in the ocean. $\Omega_{chemistry}$ is Ω calculated by Ocean Data View if there is no effect of pressure on K^*_{sp} (Ω affected only by DIC, alkalinity, salinity and temperature). $\Omega_{pressure}$ is Ω afftected by pressure, which is shown as the difference of Ω_{real} and $\Omega_{chemistry}$ here.

Above 1000 m, Fig. 1a (Ω_{real}) generally follows the trend of 1b ($\Omega_{chemistry}$), meaning that water chemistry dominates changes in Ω. $\Omega_{chemistry}$ varies between 6 at the ocean surface (not shown in the figure) and 1. Below 1000 m, Ω_{real} deviates from $\Omega_{chemistry}$ due to the effect of pressure on Ω ($\Omega_{pressure}$). At 5000 m depth, Ω can be up to 1.2 units lower than predicted by $\Omega_{chemistry}$ (Fig. 1c). The impact of $\Omega_{pressure}$ is greater in the South Pacific, somewhat less in the north, which reflects the North Pacific oxygen minimum zone's strong influence on the saturation state.

Oceanographers have assumed that carbonate dissolution under pressure follows the same dissolution rate law (same *k* and n for Eq. (2)) obtained at atmospheric pressure, with pressure only changing the stoichiometric solubility product (K^*_{sp}). In other words, a change in the denominator in Eq. (1) has the same effect as a change in the numerator in determining dissolution rates (Eq. (2)). This implies that dissolution will be kinetically the same regardless of pressure. Whether this assumption is true is the question we address in this study.

The only study, as far as we know, that examined the effect of pressure on carbonate dissolution rates versus saturation state in seawater was that of Acker et al. (1987). Their shipboard experiments measured pteropod (aragonite) dissolution rates in natural seawater at various depths between 100 and 5000 meters, based on spectrophotometric examination of seawater pH using a pH-sensitive dye, phenol red. They concluded that aragonite dissolution in seawater at variable pressures was well described by the equation $Rate = \kappa' ([CO_3^{2-}]_s - [CO_3^{2-}])^n$, where $[CO_3^{2-}]_s$ is the carbonate ion concentration at saturation, $[CO_3^{2-}]$ is the observed carbonate ion concentration, and κ' and n are empirical constants; and that their measurements were consistent with the estimate $\Delta V = -36.5 cm^3$/mole for the volume change accompanying the dissolution of aragonite. However, two factors limited the measurement precision and thus could change the interpretation of data in their study. First, dissolution rates determined from ΔpH may have a limited precision. The largest amount of dissolution in Acker et al. (1987) was only equivalent to a ΔpH~0.05; at Ω = 0.8~1, ΔpH was < 0.01. Even though the error on dissolution rates were not discussed in the paper, pH determination based on the spectrophotometric method has an error on the order of 0.002 (Robert-Baldo et al., 1985), which is greater than 20% of the

ΔpH at Ω = 0.8~1. This precision limit also arises in other seawater carbonate dissolution studies in which dissolution rates were estimated from ΔpH (e.g. Byrne et al., 1984; Gehlen et al., 2005), acid additions to keep pH constant (e.g. Walter and Morse, 1985), alkalinity change (e.g. Keir, 1980), or $CaCO_3$ dry weight loss (e.g. Peterson, 1966; Berger, 1967; Honjo and Erez, 1978; Keir, 1980; Thunell et al.,1981; Fukuhara et al., 2008). Second, shipboard experiments performed at pressures which corresponded to the depths from which the seawater samples were obtained lacked control in other key variables. Specifically, dissolution experiments were conducted under different water chemistry (carbonate system parameters) and other factors that may affect dissolution (e.g. microbial activity, soluble reactive phosphate concentrations, carbonic anhydrase activity etc.). The problem of uncontrolled variables also exists in other *in situ* seawater dissolution studies (e.g. Peterson, 1966; Berger, 1967; Milliman, 1977; Honjo and Erez, 1978; Thunell et al., 1981; Metzler et al., 1982; Fukuhara et al., 2008). The value of these earlier studies is unquestionable, yet we sought to conduct more controlled experiments to constrain the effect of pressure on calcite dissolution kinetics, focusing on Ω values closest to those most commonly encountered in the modern ocean (0.65-1).

Our goal is to distinguish the pressure effect on carbonate dissolution kinetics from the effect of water chemistry. We performed dissolution experiments in acidified Dickson standard seawater using ^{13}C labeled inorganic calcite following methodologies described in Subhas et al. (2015). This ^{13}C labeled method, coupled with tight constraints on seawater saturation state (from measurements of dissolved inorganic carbon (DIC) and total alkalinity (TA)), provides much more sensitive determinations of dissolution rates compared to previously employed methods. Desired Ω values were obtained by changing experimental pressure and/or adding HCl to the same standard Dickson seawater, so that the effect of changing pressure versus changing alkalinity on dissolution rates could be distinguished and compared. Much of the work describing $CaCO_3$ dissolution from a mechanistic perspective in this paper has built upon the foundational work of Subhas et al. (2017), and ongoing work by our group in which we investigate dissolution mechanisms as a function of temperature across a wide range of Ω values.

2. METHODS

Synthetic inorganic $Ca^{13}CO_3$ (calcite) purchased from Sigma Aldrich (SKU 492027, ≥99 atom%) was wet-sieved to a grain size of 70-100 μm using 18.2 MΩ Milli-Q water adjusted to a pH of ~8 using ammonium hydroxide. The powders were then dried at 60°C in oven overnight. The mineralogy was confirmed to be 100% calcite via XRD. Approximately 4 mg of ^{13}C labeled calcite was placed in a Supel Inert Foil Gas Sampling Bag (SUPELCO 30226-U) with 300 mL of standard reference Dickson seawater (https://www.nodc.noaa.gov/ocads/oceans/Dickson_CRM/batches.html). The Dickson standard seawater used for the dissolution experiments has a phosphate concentration of 0.28~0.58 μmol/kg. The ^{13}C calcite was placed inside a polyester mesh (41 μm mesh size) bag (Component Supply Co. /U-CMY-41-B)) to allow interaction of the solids with seawater while preventing them from leaving the system during sampling. The evolution of seawater $\delta^{13}C$ was traced over time (hours to days). $\delta^{13}C$ gain during the experiments varied from 5‰ to 50‰. $\delta^{13}C$ signals were converted into mass loss, and the dissolution rate was obtained based on the slope of moles dissolved over time. Slopes, intercepts, and the goodness of fits were obtained using the LINEST function in Microsoft Excel. Carbonate system parameters were determined by measurement of DIC and TA. $\delta^{13}C$ and DIC were determined using a Picarro Cavity Ring-Down Spectroscopy (G2131-i) coupled to a Liaison interface and a modified AutoMate autosampler. Alkalinity was determined by open-system Gran titration, performed on a custom-built instrument. All DIC and TA measurements were standardized with Dickson seawater. An in-house standard was also used to track long-term drift of the TA titration system. Characterization of materials and determination of carbonate system parameters were discussed in our previous paper in detail (Subhas et al., 2015). Ω was calculated from the CO2SYS program using the calcite partial molal volume (ΔV) reported by Ingle (1975), -37.6 $cm^3\ mol^{-1}$ at the experimental T=21°C; K'_1 K'_2 (apparent dissociation constants of carbonic acid in seawater) reported by Mehrbach et al. (1973) and refit by Dickson and Millero (1987); K_{SO_4} reported by Uppstrom (1974). Replicate precision (standard error) for DIC and TA measurements were ±1.9 μm/kg and ±1.0 μmol/kg (1σ) respectively, which allow Ω to be defined to ± 0.02.

Dissolution experiments were conducted in a custom-made pressure vessel (Fig. 2) capable of holding a sample bag at constant pressure while allowing for aliquots of the experimental

solution to be withdrawn. The pressure vessel was placed on a shaker table (VWR Standard Analog Shaker) and set to a rate of 60 rpm for all experiments. The pressure case was filled with hydraulic fluid (Lubriplate Hydraulic Jack Oil L0768-054, Lot: M0226) that was manually pumped into the pressure case around the sample bag or released from the pressure case until the system was at the desired pressure (upper limit was 5500 dbar). The sample bag was connected through a flex tubing (Altaflo PVDF Flex Tubing 14C8101, Lot: W5520-06) to a spring-loaded check valve that could "crack" at pre-set pressures, which allowed samples to be removed from the bag while pressure remained relatively constant. During sampling, a 20 mL syringe was connected to the check valve, and hydraulic fluid was slowly pumped into the pressure case to squeeze the aliquot out of the bag by increasing the pressure 20-50 dbar above the set value. Extrusion of seawater through the check valve reduced the system's volume, allowing pressure to return to the set value. Prior to sampling, the tubing and valve assembly (volume < 5 mL) was flushed by extruding 20 mL of seawater. An 8 mL sample was then injected directly into an evacuated sample vial to avoid degassing. Samples collected from a pressurized bag are referred here as *in situ*, while samples collected directly from the sample bag outside the pressure case (before and after a run) are called *ex situ*. *Ex situ* samples were taken to quantify the effect of *in situ* sampling through the tubing and check valve as artifacts may arise due to: mixing in the tubing, potential contamination from the tubing and check valve, degassing through the tubing etc. *Ex situ* rates are preferentially used because of less potential contamination, while *in situ* rate errors are used only when no obvious contamination was observed (see discussion in Supplementary Materials). The agreement between these two methods (±5%) provides confidence that our system and derived rates are free of artifact. Total moles dissolved based on both *in situ* and *ex situ* samples for one experiment (P45) are shown in Fig. 3 as an example. Potential degassing during sampling would result in lower DIC values and biased $\delta^{13}C$ (isotope fractionation during degassing) for *in situ* samples. Good agreement betweem *in situ* and *ex situ* DIC and $\delta^{13}C$ values suggests no apparent degassing while sampling. Nevertheless, for the determination of Ω based on DIC and TA, values of *ex situ* samples are used to avoid the potential contamination mentioned above.

Dissolution rates were normalized to geometric surface area (Subhas et al., 2015), which was calculated using the mean sieving size and assuming cubic geometry:

$$S.A._{geom} = \frac{6}{\rho \cdot \bar{d}} \quad (3)$$

where ρ = 2.63 g/cm^3 is the density of calcite and $\bar{d}$ is the mean grain diameter of the sieved fraction (70-100 μm).

Dissolution experiments were conducted by (i) varying pressure at fixed water chemistry (black asterisks in Fig. 4, Route 1); and (ii) varying water chemistry at fixed pressure (white circles in Fig. 4, Routes 2-6). For (ii), five sets of experiments at pressures of 10 dbar (ambient pressure), 350 dbar, 700 dbar, 1050 dbar, and 2500 dbar were conducted. 1 dbar is equivalent to 1 m ocean depth.

3. RESULTS

3.1 Dissolution rates at changing pressures

Dissolution rate measurements were made through a range of Ω values for which the change of Ω was achieved in one of two ways: by changing water chemistry (alkalinity) at atmospheric pressure (yellow squares in Fig. 5) and by changing pressure under which dissolution experiments occurred while keeping alkalinity and DIC constant (light grey circles in Fig. 5, experimental pressures are marked next to data points). In theory, both should yield similar results, but it is clear that the data are offset from one another. To get a sense of how thermodynamic uncertainty can affect the determination of Ω, the Ω's for the pressure experiments were recalculated using ΔV values that are more negative than the accepted value of -37.6 cm^{3}mol^{-1}. A change of ΔV from -37.6 cm^3 mol^{-1} (light grey circles) to -57.6 cm^3 mol^{-1} (dark grey diamonds) would make the changing pressure curve agree with the atmospheric pressure curve, but by using the conventional value of ΔV, for the same saturation state, the dissolution rate under pressure is approximately 2-4 times greater at typical oceanic Ω values of 0.8~1.0.

3.2 Dissolution rates at constant pressures

To further explore the impact of pressure on dissolution kinetics, five sets of experiments at different pressures were conducted (Fig. 6 and Table S4). For a given pressure, we adjusted the water chemistry so that a range of saturation states could be achieved. Dissolution rates increased

for the same Ω value as pressure increased from 10 dbar to 700 dbar. However, no obvious kinetic enhancement was seen when pressure was increased beyond 700 dbar up to 2500 dbar. Rate enhancement from 10 dbar to 350 dbar scaled similarly across a range of Ω from 0.9-0.65 (by a factor of approximately 1.5). The increase in rate found from 350 dbar to 700 dbar was similar (also approximately a factor of 1.5), yet, the effect of pressure on dissolution kinetics is not constant with increased pressure. This discontinuity also suggests that the pressure effect on dissolution rate is not a systematic thermodynamic error but rather a kinetic effect. This pressure effect enhances dissolution rate up to a certain pressure (approximately 700 dbar), and then ceases exerting further impact above that pressure, at least up to 2500 dbar.

3.3 Log-log correlation of dissolution rate vs. undersaturation

The formulation of Eq. 1 lends itself to an examination of values of *k* and n by plotting dissolution rates versus undersaturation. We have shown, however, in work by Subhas et al. (2015); Subhas et al. (2017); and later in this manuscript, that the values of n and *k* do not provide a mechanistic framework by which we can examine dissolution kinetics. Nevertheless, we provide this analysis to allow comparison with previous studies (Keir et al.,1980; Subhas et al., 2015).

The data for a given pressure (Fig. 7) are linearly correlated in log-log plot at lower Ω within a limited range (Zone II), but follow a different trend line closer to saturation (Zone I). The zones of different slopes are separated roughly at Ω = 0.90. Slopes of the fitting lines for 10, 350, 700, and 1050 dbar in Zone II (Ω from 0.90 to 0.50) are 3.6±0.2, 3.9±0.5, 3.1±0.3, 3.1±0.1 respectively. The slope of the log-log transformation represents the value of the empirical reaction order, n (Eq. 1). The calculated n for pressures < 1050 dbar in Zone II indicates that the observed pressure enhancement of dissolution rate does not significantly nor systematically change the reaction order.

Although dissolution kinetics are enhanced at higher pressures, there are many similarities in ambient and high-pressure dissolution phenomena. The change of slope (critical Ω) was found between Zone I and II at both ambient and high pressure. The reaction order n (slopes) for 10 dbar and 1050 dbar between Ω= 0.5 to Ω_{crit} were 3.8±0.2, 3.1±0.1 respectively; slopes for Ω >

Ω_{crit} were 0.47±0.27 and 0.46±0.15. The critical point for both pressure conditions was within the error of each other; Ω_{crit} is 0.87±0.05 at 10 dbar; and 0.90±0.03 at 1050 dbar. We note that this Ω_{crit} is a different critical undersaturation point for calcite dissolution in seawater from that reported by Subhas et al. (2017) (Ω=0.7) and other researchers (e.g. Berner and Morse, 1974, Ω=0.67). This study is the first study to get close enough to equilibrium, because of the high sensitivity of rate measurements using our ^{13}C labeling technique, to see a Ω_{crit} at 0.87~0.90. The implicit meaning of the two different Ω_{crit} will be discussed in section 4.2.

4. DISCUSSION

4.1 Thermodynamic uncertainty and Partial Molal Volume

According to our results, a significant difference in dissolution rate vs. undersaturation exists between varying water chemistry and varying pressure (Fig. 5). This discrepancy can either be due to uncertainty in values of undersaturation, or real differences in rate at fixed saturation state. If the former is true, the degree of undersaturation under pressure may have an error related to the uncertainty in the Partial Molal Volume, ΔV, of the dissolution reaction. If the latter is true, our results can be interpreted as a real pressure effect on dissolution rate, above and beyond its effect on thermodynamics.

The effect of pressure on thermodynamic constants can be determined in two ways (Millero, 1995): (1) using direct measurements of the constants (Culberson and Pytkowicz, 1968) and (2) using partial molal volume and compressibility data (Millero, 1979, 1983). The two methods have been shown to be in good agreement (Millero, 1979). The effect of pressure on the dissociation constants of acids (K_i) can be made from (Millero, 1979) equations of the form:

$$ln\left(\frac{K_i^P}{K_i^O}\right) = -\left(\frac{\Delta V_i}{RT}\right)P + \left(0.5\frac{\Delta \kappa_i}{RT}\right)P^2 \quad (4)$$

where P is the applied pressure in bars, and ΔV_i and $\Delta\kappa_i$ are the molal volume and compressibility change for the association or dissociation reactions. The values of ΔV_i and $\Delta\kappa_i$ for the ionization of acids have been fit to equations of the form for seawater of S=35:

$$\Delta V_i = a_0 + a_1 t + a_2 t^2; \quad (5)$$

$$\Delta \kappa_i = b_0 + b_1 t + b_2 t^2. \quad (6)$$

where t is temperature in °C. The coefficients in Eq. (5) and (6) for the dissociation of H_2CO_3, HCO_3^-, $CaCO_3$ (calcite), $CaCO_3$ (aragonite) are given in Table 1 (Culberson and Pytkowicz, 1968; Ingle, 1975).

The effect of pressure on the solubility of calcite (K^*_{sp}) was measured and reviewed in Ingle (1975) (Table 2). At 25°C, reported $\Delta V_{calc.}$ varied by about 20% (-39.4 to -31.8 $cm^3\ mol^{-1}$, $\Delta V_{calc.}$ obtained as pressure was increased from 1 to 1000 atm). Due to the small discrepancies in $\Delta V_{calc.}$ values reported by different researchers, these $\Delta V_{calc.}$ expressions and values have been widely used since 1970s. CO2SYS (v1.1, 2011), the program we used to calculate carbonate system variables, adopts parameters from Ingle (1975) and Millero (1979), and determines calcite ΔV_i with the equation:

$$\Delta V_i = -48.76 + 0.5304t \quad (7)$$

which yielded -35.5 $cm^3\ mol^{-1}$ at 25°C, and -37.6 $cm^3\ mol^{-1}$ at 21°C.

If the difference between ambient and higher pressure experimental dissolution rates is due to an inaccurate $\Delta V_{calc.}$ value, then an adjustment of $\Delta V_{calc.}$ at 21°C from -37.6 $cm^3\ mol^{-1}$ to -57.6 $cm^3\ mol^{-1}$ is necessary to make the two results agree (Fig. 5). The uncertainty (±20%) in partial molar volume based on previous research does not support the almost factor of two change in $\Delta V_{calc.}$ necessary to align our ambient and high-pressure data sets.

This change in calcite $\Delta V_{calc.}$ is also approximately equivalent to a change of $\Delta V(H_2CO_3)$ (pressure effect on K_1) at 21°C from -22.8 $cm^3\ mol^{-1}$ to -59.3 $cm^3\ mol^{-1}$; or a change of $\Delta V(HCO_3^-)$ (pressure effect on K_2) at 21°C from -16.3 $cm^3\ mol^{-1}$ to 12.0 $cm^3\ mol^{-1}$, both of which seem unreasonable. Therefore, we believe that dissolution under higher pressure is a true kinetic effect. Previous work by Subhas et al. (2015) yield similar ambient pressure data as we

obtained, hence we believe the low-pressure work is reproducible and the difference we see between different pressures is real.

4.2 Different dissolution mechanisms and critical degree of undersaturation

Dissolution and crystal growth are usually considered complementary processes, and are thus linked in terms of mechanisms. The earliest mechanistic studies on mineral dissolution can be traced back to the well-established BCF theory (Burton et al., 1951; Cabrera et al., 1954; Cabrera and Levine, 1956). According to the BCF theory, a critical free energy value is required to open etch pits at line defects such as screw dislocations. Only if this critical value is reached can pre-existing hollow cores (Frank, 1951) open up into etch pits. Lasaga and Lüttge (2001, 2003) further introduced the stepwave model, explaining that the pit walls are the source for steps that emanate from the outskirts of the pits and travel across the crystal surface. In contrast, at near-equilibrium conditions, the difference in free energy is insufficient for hollow cores to open into pits; the critical source for stepwaves is therefore missing. Near equilibrium, the dissolution mechanism is driven primarily by point defects and dissolution on pre-existing edges and corners, and advances as step edge retreats, a much slower process than the stepwave mechanism (Arvidson and Lüttge, 2010).

Dissolution experiments of various minerals have shown discontinuities in the function of dissolution rate versus the distance from equilibrium. These minerals include carbonates (Berner and Morse, 1974; Pokrovsky and Schott, 1999; Pokrovsky and Schott, 2001; Teng, 2004; Pokrovsky et al., 2009; Lüttge and Arvidson, 2010; Xu et al., 2012; Subhas et al., 2017), silicates (Knauss and Wolery, 1986; Nagy et al., 1991; Burch et al., 1993; Gautier et al., 1994; Ganor et al., 1995; Oelkers et al., 1994; Devidal et al., 1997; Oelkers and Schott, 1999; Taylor et al., 2000; Dove et al., 2005; Hellmann and Tisserand, 2006; Arvidson and Lüttge, 2010), and others (Nagy and Lasaga, 1992; Pokrovsky and Schott, 2004). For calcite dissolution in seawater, Berner and Morse (1974) related the "near-equilibrium criticality" to the abundance of phosphate ion absorbed to the mineral surface. They hypothesized that these adsorbed ions prevent dissolution steps from propagating. Once below a certain threshold saturation state ($\Delta pH=0.10$, $\Omega=0.67$ for calcite in seawater), monomolecular steps on the crystal surface can penetrate between adsorbed inhibiting phosphate ions. The presence of the chemical lysocline in the oceans was believed to

be due to this mechanism. Direct observations of crystal surfaces with Vertical Scanning Inferometry and Atomic Force Microscopy have linked observed rate discontinuities with the activation of different crystal surface features (Teng, 2004; Beig and Lüttge, 2006; Lüttge, 2006; Xu et al., 2010; Xu et al., 2012; Schott et al., 2012). Based on AFM observations, Teng (2004) reported a Ω_{crit} = 0.54 for calcite step-edge propagation (opening up of etch pits) in freshwater, whereas Xu et al. (2012) observed the first appearance of etch pits at Ω = 0.904. This Ω_{crit} was correlated with an abrupt change in velocity of obtuse steps instead of acute steps (Xu et al., 2010, Ω ≈ 0.8). Subhas et al. (2017) reported a Ω_{crit}= 0.70~0.75 in seawater, between defect-assisted dissolution mechanism and the homogeneous spreading of etch pits, by plotting lab dissolution rate of calcite in seawater within the mechanistic framework proposed by Dove et al. (2005), as briefly described below.

Our work confirms a discontinuity of dissolution behavior much closer to equilibrium, as defined by the change of slope in log(rate) vs. log(undersaturation) plots (Fig. 7). Linear fits change slope at log(1- Ω) > -0.9, which is equivalent to Ω_{crit} of around 0.9. As noted previously, the influence of pressure does not change the value of Ω_{crit}. Below, we investigate the significance of dissolution rates under ambient and higher pressures by organizing the data, rather than by n and *k*, but within the mechanistic framework proposed by Dove et al. (2005). By reorganizing equations in Dove et al. (2005) to describe dissolution, for homogenous or defect-assisted dissolution we find:

$$ln\left(\frac{|Rate|}{(1-\Omega)^{\frac{2}{3}}|\sigma|^{\frac{1}{6}}}\right) = ln\left(h\beta C_e(\omega^2 h n_s a)^{\frac{1}{3}}\right) - \frac{\pi\alpha^2\omega h}{3(k_b T)^2}\left|\frac{1}{\sigma}\right| \quad (8)$$

where *Rate* is the normalized dissolution velocity (m/s), $|\sigma| = \ln(\Omega)$, *h* is the step height (nm), β is the step kinetic coefficient (cm/s), C_e is the equilibrium concentration of dissolved species in solution (molecules/m^3), ω is the molecular volume (cm^3), n_s is the density of pit nucleation sites, *a* is lattice spacing (m), α is the interfacial free energy (mJ/m^2), k_b is the Boltzman Constant, *T* is absolute temperature (K). As given by this formulation, the dissolution rate should be a linear function of $\left|\frac{1}{\sigma}\right|$ and the slope should be negative.

For the step retreat mechanism, which occurs closer to equilibrium, the dissolution rate function is not linear with $\left|\frac{1}{\sigma}\right|$:

$$ln\left(\frac{|Rate|}{(1-\Omega)^{\frac{2}{3}}|\sigma|^{\frac{1}{6}}}\right) = ln\left(\frac{\omega\beta C_e m\hbar}{P}\right) + ln\left((1-\Omega)^{\frac{1}{3}}\left|\frac{1}{\sigma}\right|^{\frac{1}{6}}\right) - ln\,(1+8\left(\frac{\omega\alpha}{Pk_bT}\right)\left|\frac{1}{\sigma}\right|) \quad (9)$$

Therefore, by plotting lab-derived dissolution rate data in this framework and interrogating its trends, we can demonstrate a shift from the step-retreat dissolution mechanism near equilibrium to the defect-assisted mechanism farther from equilibrium for calcite dissolution in seawater (Fig. 8). In Zone II ($\left|\frac{1}{\sigma}\right|$<9), $ln\left(\frac{|Rate|}{(1-\Omega)^{\frac{2}{3}}|\sigma|^{\frac{1}{6}}}\right)$ decreases as $\left|\frac{1}{\sigma}\right|$ increases, and the relationship is linear, as predicted by Eq. (8). In Zone I ($\left|\frac{1}{\sigma}\right|$>9), data points fall off the linear trends with negative slopes and $ln\left(\frac{|Rate|}{(1-\Omega)^{\frac{2}{3}}|\sigma|^{\frac{1}{6}}}\right)$ increases slightly with increasing $\left|\frac{1}{\sigma}\right|$, as predicted by Eq. (9). A closer examination of the Zone II data reveals that there may be two different negative slopes representing homogenous and defect-assisted dissolution respectively, but our data are not dense enough, especially far from equilibrium (low $\left|\frac{1}{\sigma}\right|$) to see this conclusively. Closer to equilibrium, the transition between defect-assisted and step-retreat dissolution mechanisms (boundary of Zone II and I) occurs at $\left|\frac{1}{\sigma}\right|$ = 8~9, which is equivalent to Ω= 0.88~0.89, consistent with Ω_{crit} determined in log-log plots (Fig. 7). Although, the Ω_{crit} does not appear to be sensitive to pressure, the slopes at different pressures in Zone II (Fig. 8) indicate a change of the local interfacial energy barrier, α (Fig. 9a and Table 3). The energy barrier α decreases as pressure increases, but this decrease appears to level off at ~700 dbar. The intercept of the Zone II slope in Fig. 8 provides information about two other parameters in Eq. 8. Increasing pressure does not seem to significantly change the intercept (Fig. 9b), which means that the density of nucleation sites (n_s) and/or the velocity of step retreat (β) are similar.

These results suggest that increased pressure may lower the interfacial energy barrier at the calcite-seawater interface, resulting in enhanced dissolution kinetics. This effect may result from pressure-dependent speciation changes in seawater surrounding the mineral surface, and/or changes in bonding energy between ions in seawater and the mineral surface. The changes in speciation and/or bonding energy take place as pressure increases from ambient pressure to 700 dbar, but become complete at ~700 dbar. Conversely, the number of nucleation sites for dissolution and/or the velocity of step retreat do not appear to change with pressure. How exactly pressure affects the surface energy of calcite is still an open question, yet a deeper understanding of calcite dissolution kinetics will require delving into this particular phenomenon.

Combined with the results from Subhas et al. (2017), we report distinct and robust mechanism transitions for calcite dissolution in seawater from step-retreat to defect-assisted dissolution, and further to an etch pit spreading mechanism. The two Ω_{crit} values were shown to be ~0.9 for the former transition, and ~0.75 for the latter transition. Our ^{13}C labeling method has allowed us high enough sensitivity at slow dissolution rates to determine the Ω_{crit} between the step retreat mechanism and the defect-assisted mechanism, and both mechanisms are in evidence at ambient pressure and as pressure increases.

4.3 Effect of pressure on shallow water column carbonate dissolution

Although estimates of carbonate production in the surface, open ocean vary (0.4-2 Gt/yr) (e.g. Milliman, 1993; Milliman, 1999; Balch and Kilpatrick, 1996; Balch et al., 2007; Dunne et al., 2007; Dunne et al., 2012 etc.), it has been recognized that carbonate production in the ocean well exceeds the amount of carbonate burial (Sarmiento and Gruber, 2006; Berelson et al., 2007). Battaglia et al. (2015) reported median global $CaCO_3$ export to be 0.82 Gt PIC/yr (within the lower half of previously published estimates (0.4-1.8 Gt PIC/yr), where PIC is Particulate Inorganic Carbon); and that only 29% reaches the seafloor. These studies of global carbonate flux have set up a problem in global geochemistry which has yet to be resolved—how much carbonate is dissolving in the open ocean water column and what factors control the dissolution rate.

Water column shallow-depth $CaCO_3$ dissolution (SDCCD) has been recognized by several independent studies (e.g. Anderson and Sarmiento, 1994; Lohmann, 1995; Milliman and Droxler, 1996; Milliman et al., 1999; Chen et al., 2002; Schiebel, 2002; Gangstø et al., 2008), and could account for some of the discrepancy between carbonate production and sediment-trap flux estimates mentioned above. Conventional wisdom is that calcium carbonate shells are dissolved when they reach the saturation horizon of aragonite or calcite during sinking, which provides the alkalinity that can be supplied back to the surface ocean via upwelling/diapycnal mixing. However, researchers have shown significant dissolution above the "saturation horizons" (Feely et al., 2002; Gangstø et al., 2008). The impact of the SDCCD finding is that it implies a shorter time scale for the cycling of calcium carbonate within the ocean. This would have implications for feedbacks between climate, atmospheric CO_2, and the marine carbon cycle.

Possible mechanisms responsible for SDCCD were proposed to include (1) dissolution of $CaCO_3$ particles in the guts of zooplankton (Takahashi, 1975; Bishop et al., 1980, 1986; Van der Wal et al., 1995; White et al., 2016), even though others provide some skepticism regarding this mechanism (Harris, 1994; Pond et al., 1995); (2) dissolution of $CaCO_3$ particles in microenvironments where bacterial oxidation of organic matter can enhance the dissolution process (Jansen et al., 2002); (3) dissolution of the more soluble forms of $CaCO_3$ in shallow waters, including aragonite and high-Mg calcites (Byrne et al., 1984; Morse and Mackenzie, 1990); (4) the source of excess alkalinity for subsurface waters in the open ocean is from the decomposition of organic matter occurring in shelf sediments (Chen, 2002; Burt et al., 2016), or transport/mixing subsequent to dissolution (Friis et al., 2006, 2007), and hence there is not evidence of SDCCD.

Whereas the pressure effect on inorganic calcite dissolution described in this paper is beyond doubt, the direct application of the rate law to illustrate carbonate dissolution patterns in the ocean remains to be tested. Sinking calcite particles are "ballasted" within fecal pellets, "snow" and other aggregates (Honjo, 1980, 1995; Honjo et al., 1982; Armstrong et al., 2001; Klaas and Archer, 2002), which will complicate the process of dissolution while sinking by (1) enhancing settling velocity by orders of magnitude (Armstrong et al., 2009), (2) lowering PIC reactivity by providing physical protection (Armstrong et al., 2001), (3) providing locally acidic environments

through bacterial oxidation of organic matter (Jansen et al., 2002), etc. Rates of carbonate dissolution at the seafloor, on the other hand, are further complicated by boundary layer processes between sediments and the overlying seawater (Boudreau, 1982, 2001, 2013; Sulpis et al., 2017). Nevertheless, the revised dissolution rate formulation as a function of pressure should be taken into consideration in future marine carbon cycle studies. It will also be interesting to investigate the effect of pressure on other minerals, including the more soluble forms of $CaCO_3$ (e.g. aragonite and high-Mg calcite). We believe that previous water column dissolution rate measurements of $CaCO_3$ (calcite and possibly other carbonate minerals) were underestimated, and this pressure effect can account, at least partially, for the observed ocean production-burial discrepancy.

5. CONCLUSIONS

We have presented experiments demonstrating elevated dissolution rates of calcite in seawater under high pressure compared to equivalent undersaturation states under ambient pressure. This enhancement was observed over an Ω range of 0.65 to 1. The discrepancy of dissolution behavior under different pressures is greater than the uncertainty of Ω based on uncertainties in ΔV, and is therefore attributed to a pressure effect on the dissolution rate itself. This kinetic pressure enhancement effect takes place relatively evenly between ambient pressure to 700 dbar, but ceases at pressures above 700 dbar (pressures higher than 700 dbar yield dissolution rates similar to rates at 700 dbar, at least up to 2500 dbar). The calcite dissolution rates in seawater at 700 dbar is 2-4 times faster than at ambient pressure. Dissolution rates at different pressures share the same reaction order n in Rate=$k(1-\Omega)^n$. Furthermore, a discontinuity in the functional relationship between dissolution rate and undersaturation indicates a change of the rate-controlling dissolution mechanism at values of $\Omega_{critical}$. We interpret this $\Omega_{critical}$ to be the threshold between a step-retreat dissolution mechanism and a defect-assisted mechanism. $\Omega_{critical}$ at 10 dbar and 1050 dbar are similar, 0.87±0.05 and 0.90±0.03 respectively. The reaction order n above $\Omega_{critical}$ is ~0.5, and ~3.4 below $\Omega_{critical}$. By transforming dissolution rate vs. saturation state into an equation (Eq. 8) that includes mechanistic information, we find that the effect of pressure is to lower the surface energy barrier to dissolution. The enhanced pressure-related dissolution of carbonate minerals may explain excess alkalinity distributions in the ocean as this would effectively decrease the depth at which rapid dissolution occurs.

ACKNOWLEDGEMENTS

This work was supported by NSF Ocean Acidification grants (numbers OCE1220600 and OCE1220302), USC Dornsife Doctoral Fellowship and Elizabeth and Jerol Sonosky Fellowship for Earth and Ocean Sciences. The authors would like to thank Jun Shao for helping with Fig. 1 in this paper using Ocean Data View. We acknowledge the work by USC machine shop machinists (Don Wiggins and colleagues) who built our pressure vessel and undergraduate student Laura Morine for her help running alkalinities. We also thank Dr. Alfonso Mucci, Dr. Bernard Boudreau, and two anonymous reviewers for their valuable and constructive comments on the original manuscript draft.

REFERENCES

Acker, J. G., Byrne, R. H., Ben-Yaakov, S., Feely, R. A., & Betzer, P. R. (1987) The effect of pressure on aragonite dissolution rates in seawater. *Geochimica et Cosmochimica Acta*, *51*(8), 2171-2175.

Anderson, L. A. and Sarmiento, J. L. (1994) Redfield ratios of remineralization determined by nutrient data analysis, *Global Biogeochem. Cycles, 8, 65–80*.

Armstrong, R. A., Lee, C., Hedges, J. I., Honjo, S., & Wakeham, S. G. (2001). A new, mechanistic model for organic carbon fluxes in the ocean based on the quantitative association of POC with ballast minerals. *Deep Sea Research Part II: Topical Studies in Oceanography, 49(1-3), 219-236.*

Armstrong, R. A., Peterson, M. L., Lee, C., & Wakeham, S. G. (2009). Settling velocity spectra and the ballast ratio hypothesis. *Deep Sea Research Part II: Topical Studies in Oceanography, 56(18), 1470-1478.*

Arvidson, R. S., & Lüttge, A. (2010) Mineral dissolution kinetics as a function of distance from equilibrium–New experimental results. *Chemical geology*, *269*(1), 79-88.

Balch, W. M., and K. A. Kilpatrick (1996) Calcification rates in the equatorial Pacific along 140_W, *Deep Sea Res., Part II, 43, 971– 993.*

Balch, W. M., D. T. Drapeau, B. C. Bowler, and E. Booth (2007) Prediction of pelagic calcification rates using satellite-measurements, *Deep Sea Res., Part II, Vol. 54, Issues 5-7, Pages 478-495, doi: 10.1016/j.dsr2.2006.12.006*

Battaglia, G., Steinacher, M., & Joos, F. (2015) A probabilistic assessment of calcium carbonate export and dissolution in the modern ocean. *Biogeosciences Discussions*, *12(24).*

Beig, M. S., & Lüttge, A. (2006) Albite dissolution kinetics as a function of distance from equilibrium: Implications for natural feldspar weathering. *Geochimica et Cosmochimica Acta*, *70*(6), 1402-1420.

Berelson W.M., Balch W.M., Najjar R., Feely R.A., Sabine C., Lee K. (2007) Relating estimates of $CaCO_3$ production, export, and dissolution in the water column to measurements of $CaCO_3$ rain into sediment traps and dissolution on the sea floor: A revised global carbonate budget. *Global Biogeochem. Cycles, Vol. 20, GB1024, doi:10.1029/2006GB002803.*

Berger, W. H. (1967) Foraminiferal ooze: solution at depths. *Science*, *156*(3773), 383-385.

Berner, R. A., & Morse, J. W. (1974) Dissolution kinetics of calcium carbonate in sea water; IV, Theory of calcite dissolution. *American Journal of Science*, *274*(2), 108-134.

Bishop, J. K. B., J. C. Stepien, and P. H. Weibe (1986) Particulate matter distributions, chemistry and fluxes in the Panama Basin: Response to environmental forcing, *Prog. Oceanogr., 17, 1– 59.*

Bishop, J. K. B., R. W. Collier, D. R. Kettens, and J. M. Edmond (1980) The chemistry, biology and vertical flux of particulate matter from the upper 1500 m of the Panama Basin, *Deep Sea Res., Part I, 27, 615– 640*.

Boudreau, B. P. (1982). The influence of a diffusive sublayer on accretion, dissoluton, and diagenesis at the sea floor. *The dynamic environment of the ocean floor.*

Boudreau, B. P. (2001). Solute transport above the sediment-water interface. *The Benthic boundary layer: Transport processes and biogeochemistry, 104-126.*

Boudreau, B. P. (2013). Carbonate dissolution rates at the deep ocean floor. *Geophysical Research Letters, 40(4), 744-748.*

Burch, T. E., Nagy, K. L., & Lasaga, A. C. (1993) Free energy dependence of albite dissolution kinetics at 80 C and pH 8.8. *Chemical Geology, 105*(1-3), 137-162.

Burt, W. J., Thomas, H., Hagens, M., Pätsch, J., Clargo, N. M., Salt, L. A., ... & Böttcher, M. E. (2016). Carbon sources in the North Sea evaluated by means of radium and stable carbon isotope tracers. *Limnology and Oceanography, 61*(2), 666-683.

Burton, W. K., Cabrera, N., & Frank, F. C. (1951) The growth of crystals and the equilibrium structure of their surfaces. *Philosophical Transactions of the Royal Society of London A: Mathematical, Physical and Engineering Sciences, 243*(866), 299-358.

Byrne, R. H., J. G. Acker, P. R. Betzer, R. A. Feely, and M. H. Cates (1984) Water column dissolution of aragonite in the Pacific Ocean, *Nature, 312, 321– 326*.

Cabrera, N., & Levine, M. M. (1956) XLV. On the dislocation theory of evaporation of crystals. *Philosophical Magazine, 1*(5), 450-458.

Cabrera, N., Levine, M. M., & Plaskett, J. S. (1954) Hollow dislocations and etch pits. *Physical Review, 96*(4), 1153.

Chen, C.-T. A. (2002) Shelf-vs. dissolution-generated alkalinity above the chemical lysocline, *Deep Sea Res., Part II, 49, 5365– 5375*.

Chernov, A.A. (1984) Modern Crystallography III: Crystal Growth, Springer Science & Business Media.

Culberson, C., & Pytkowicx, R. M. (1968) Effect of pressure on carbonic acid, boric acid, and the pH 1N seawater. *Limnology*.

Devidal, J. L., Schott, J., & Dandurand, J. L. (1997) An experimental study of kaolinite dissolution and precipitation kinetics as a function of chemical affinity and solution composition at 150 C, 40 bars, and pH 2, 6.8, and 7.8. *Geochimica et Cosmochimica Acta, 61(24), 5165-5186.*

Dickson, A.G., Millero, F.J. (1987) A comparison of the equilibrium constants for the dissociation of carbonic acid in seawater media. *Deep Sea Research Part A, Oceanographic Research Papers. 34, 1733-1743.*

Dove, P. M., Han, N., & De Yoreo, J. J. (2005) Mechanisms of classical crystal growth theory explain quartz and silicate dissolution behavior. *Proceedings of the National Academy of Sciences, 102(43), 15357-15362.*

Duedall, I. W. (1972) The partial molal volume of calcium carbonate in sea water. *Geochimica et Cosmochimica Acta*, *36*(7), *729-734.*

Dunne, J. P., B. Hales, and J. R. Toggweiler (2012) Global calcite cycling constrained by sediment preservation controls, *Global Biogeochem. Cycles, 26, GB3023, doi:10.1029/2010GB003935.*

Dunne, J. P., J. L. Sarmiento, and A. Gnanadesikan (2007) A synthesis of global particle export from the surface ocean and cycling through the ocean interior and on the seafloor, *Global Biogeochem. Cycles, 21, GB4006, doi:10.1029/2006GB002907.*

Feely R.A., Sabine C.L., Lee K., Millero F.J., Lamb M.F., Greeley D., Bullister J.L., Key R.M., Peng T.-H., Kozyr A., Ono T., Wong C.S. (2002) *In situ* calcium carbonate dissolution in the Pacific Ocean. *Global Biogeochemical Cycles. Vol. 16, No. 4, 1144, doi:10.1029/2002GB001866, 2002.*

Frank, F. C. (1951) Capillary equilibria of dislocated crystals. *Acta Crystallographica*, *4*(6), 497-501.

Friis K., Najjar R.G., Follows M.J., Dutkiewicz S. (2006) Possible overestimation of shallow-depth calcium carbonate dissolution in the ocean. *Global Biogeochem. Cycles, 20, GB4019, doi:10.1029/2006GB002727.*

Friis, K., R. G. Najjar, M. J. Follows, S. Dutkiewicz, A. Kortzinger, and K. M. Johnson (2007) Dissolution of calcium carbonate: Observations and model results in the North Atlantic, *Biogeosciences, 4. pp. 205-213. DOI 10.5194/bg-4-205-2007.*

Fukuhara, T., Tanaka, Y., Ioka, N., & Nishimura, A. (2008) An *in situ* experiment of calcium carbonate dissolution in the central Pacific Ocean. *International Journal of Greenhouse Gas Control*, *2*(1), 78-88.

Gangstø, R., Gehlen, M., Schneider, B., Bopp, L., Aumont, O., & Joos, F. (2008) Modeling the marine aragonite cycle: changes under rising carbon dioxide and its role in shallow water $CaCO_3$ dissolution. *Biogeosciences,5(4), 1057-1072.*

Ganor, J., Mogollón, J. L., & Lasaga, A. C. (1995) The effect of pH on kaolinite dissolution rates and on activation energy. *Geochimica et Cosmochimica Acta*, *59*(6), 1037-1052.

Gautier, J. M., Oelkers, E. H., & Schott, J. (1994) Experimental study of K-feldspar dissolution rates as a function of chemical affinity at 150 C and pH 9. *Geochimica et Cosmochimica Acta*, *58*(21), 4549-4560.

Gehlen, M., Bassinot, F. C., Chou, L., & McCorkle, D. (2005) Reassessing the dissolution of marine carbonates: II. Reaction kinetics. *Deep Sea Research Part I: Oceanographic Research Papers*, *52*(8), 1461-1476.

Hales, B., & Emerson, S. (1997). vidence in support of first-order dissolution kinetics of calcite in seawater. Earth and Planetary Science Letters, 148(1-2), 317-327.

Harris, R. P. (1994) Zooplankton grazing on the coccolithophore Emiliani huxleyi and its role in the inorganic carbon flux, *Mar. Biol., 119, 431–439.*

Hawley, J., & Pytkowicz, R. M. (1969) Solubility of calcium carbonate in seawater at high pressures and 2 C. *Geochimica et cosmochimica acta*,*33*(12), 1557-1561.

Hellmann, R., & Tisserand, D. (2006) Dissolution kinetics as a function of the Gibbs free energy of reaction: An experimental study based on albite feldspar. *Geochimica et Cosmochimica Acta*, *70*(2), 364-383.

Honjo, S. (1980). Material fluxes and modes of sedimentation in the mesopelagic and bathypelagic zones. *J. mar. Res., 38, 53-97.*

Honjo, S., & Erez, J. (1978) Dissolution rates of calcium carbonate in the deep ocean; an in-situ experiment in the North Atlantic Ocean. *Earth and Planetary Science Letters*, *40*(2), 287-300.

Honjo, S., Dymond, J., Collier, R., & Manganini, S. J. (1995). Export production of particles to the interior of the equatorial Pacific Ocean during the 1992 EqPac experiment. *Deep Sea Research Part II: Topical Studies in Oceanography, 42(2-3), 831-870.*

Honjo, S., Manganini, S. J., & Cole, J. J. (1982). Sedimentation of biogenic matter in the deep ocean. *Deep Sea Research Part A. Oceanographic Research Papers, 29(5), 609-625.*

Ingle, S. E. (1975) Solubility of calcite in the ocean. *Marine Chemistry*, 3(4), 301-319.

Jansen H., Zeebe R.E., Wolf-Gladrow D.A. (2002) Modeling the dissolution of settling $CaCO_3$ in the ocean. *Global Biogeochemical Cycles, Vol. 16, No. 2, 1027, 10.1029/2000GB001279, 2002.*

Keir, R. S. (1980) The dissolution kinetics of biogenic calcium carbonates in seawater. *Geochimica et Cosmochimica Acta, 44*(2), 241-252.

Klaas, C., & Archer, D. E. (2002). Association of sinking organic matter with various types of mineral ballast in the deep sea: Implications for the rain ratio. *Global Biogeochemical Cycles, 16(4).*

Knauss, K. G., & Wolery, T. J. (1986) Dependence of albite dissolution kinetics on pH and time at 25 C and 70 C. *Geochimica et Cosmochimica Acta, 50*(11), 2481-2497.

Lasaga, A. C., & Lüttge, A. (2001) Variation of crystal dissolution rate based on a dissolution stepwave model. *Science, 291*(5512), 2400-2404.

Lasaga, A. C., & Lüttge, A. (2003) A model for crystal dissolution. *European Journal of Mineralogy, 15*(4), 603-615.

Lohmann, G. P. (1995) A model for variation in the chemistry of planktonic foraminifera due to secondary calcification and selective dissolution, *Paleoceanography, 10, 445–457.*

Lüttge, A. (2006) Crystal dissolution kinetics and Gibbs free energy. *Journal of Electron Spectroscopy and Related Phenomena, 150*(2), 248-259.

Lüttge, A., & Arvidson, R. S. (2010). Reactions at surfaces: A new approach integrating interferometry and kinetic simulations. *Journal of the American Ceramic Society, 93(11), 3519-3530.*

Malkin, A.I., Chernov, A.A., Alexeev, I.V. (1989) Growth of Dipyramidal face of dislocation-free ADP crystals; free energy of steps. *Journal of Crystal Growth, 97, pp. 765-769.*

Mehrbach, C., Culberson, C., Hawley J.E., Pytkowicz R.M. (1973) Measurement of the apparent dissociation constants of carbonic acid in seawater at atmospheric pressure. *Limnology and Oceanography, 18, 897–907.*

Metzler, C. V., Wenkam, C. R., & Berger, W. H. (1982) Dissolution of foraminifera in the eastern equatorial Pacific; an *in situ* experiment. *Journal of Foraminiferal Research*, *12*(4), 362-368.

Millero, F. J. (1979) The thermodynamics of the carbonate system in seawater. *Geochimica et Cosmochimica Acta*, *43*(10), 1651-1661.

Millero, F. J. (1983) The estimation of the pK* HA of acids in seawater using the Pitzer equations. *Geochimica et Cosmochimica Acta*, *47*(12), 2121-2129.

Millero, F. J. (1995) Thermodynamics of the carbon dioxide system in the oceans. *Geochimica et Cosmochimica Acta*, *59*(4), 661-677.

Millero, F. J., & Berner, R. A. (1972) Effect of pressure on carbonate equilibria in seawater. *Geochimica et Cosmochimica Acta*, *36*(1), 92-98.

Milliman, J. D. (1978) *Dissolution of calcium carbonate in the Sargasso Sea (Northwest Atlantic)*. Woods Hole Oceanographic Institution.

Milliman, J. D. (1993) Production and accumulation of calcium carbonate in the ocean: Budget of a nonsteady state, *Global Biogeochem. Cycles, 7, 927– 957.*

Milliman, J. D. and Droxler, A. W. (1996) Neritic and pelagic carbonate sedimentation in the marine environment: Ignorance is not bliss, *Geologische Rundschau, 85(3), 496–504.*

Milliman, J. D., P. J. Troy, W. M. Balch, A. K. Adams, Y.-H. Li, and F. T. MacKenzie (1999) Biologically-mediated dissolution of calcium carbonate above the chemical lysocline? *Deep Sea Res., Part I, 46, 1653–1669.*

Morse, J. W. (1978) Dissolution kinetics of calcium carbonate in sea water: VI. The near-equilibrium dissolution kinetics of calcium carbonate-rich deep sea sediments. *Am. J. Sci.;(United States)*, *278*(3).

Morse, J. W., and F. T. Mackenzie (1990) Geochemistry of sedimentary carbonates, *707 pp., Elsevier Sci., New York*.

Morse, J. W., de Kanel, J. O. H. N., & Harris, K. A. R. E. N. (1979) Dissolution kinetics of calcium carbonate in seawater; VII, The dissolution kinetics of synthetic aragonite and pteropod tests. *American Journal of Science*, *279*(5), 488-502.

Mucci, A. (1983) The solubility of calcite and aragonite in seawater at various salinities, temperatures, and one atmosphere total pressure. *American Journal of Science*, *283*(7), 780-799.

Nagy, K. L., & Lasaga, A. C. (1992) Dissolution and precipitation kinetics of gibbsite at 80 C and pH 3: The dependence on solution saturation state. *Geochimica et Cosmochimica Acta*, *56*(8), 3093-3111.

Nagy, K. L., Blum, A. E., & Lasaga, A. C. (1991) Dissolution and precipitation kinetics of kaolinite at 80 degrees C and pH 3; the dependence on solution saturation state. *American Journal of Science*, *291*(7), 649-686.

Oelkers, E. H., & Schott, J. (1999) Experimental study of kyanite dissolution rates as a function of chemical affinity and solution composition. *Geochimica et Cosmochimica Acta*, *63*(6), 785-797.

Oelkers, E. H., Schott, J., & Devidal, J. L. (1994) The effect of aluminum, pH, and chemical affinity on the rates of aluminosilicate dissolution reactions. *Geochimica et Cosmochimica Acta*, *58*(9), 2011-2024.

Peterson, M. N. A. (1966) Calcite: rates of dissolution in a vertical profile in the central Pacific. *Science*, *154*(3756), 1542-1544.

Pokrovsky, O. S., & Schott, J. (1999) Processes at the magnesium-bearing carbonates/solution interface. II. kinetics and mechanism of magnesite dissolution. *Geochimica et cosmochimica acta*, *63*(6), 881-897.

Pokrovsky, O. S., & Schott, J. (2001) Kinetics and mechanism of dolomite dissolution in neutral to alkaline solutions revisited. *American Journal of Science*, *301*(7), 597-626.

Pokrovsky, O. S., & Schott, J. (2004) Experimental study of brucite dissolution and precipitation in aqueous solutions: surface speciation and chemical affinity control. *Geochimica et Cosmochimica Acta*, *68*(1), 31-45.

Pokrovsky, O. S., Golubev, S. V., Schott, J., & Castillo, A. (2009) Calcite, dolomite and magnesite dissolution kinetics in aqueous solutions at acid to circumneutral pH, 25 to 150 C and 1 to 55 atm pCO_2: New constraints on CO_2 sequestration in sedimentary basins. *Chemical geology*, *265*(1), 20-32.

Pond, D. W., R. P. Harris, and C. A. Brownlee (1995) Microinjection technique using a pH sensitive dye to determine the gut pH of Calanus helgolandicus. *Mar. Biol., 123, 75–79.*

Pytkowicz, R. M., & Fowler, G. A. (1967) Solubility of foraminifera in seawater at high pressures. *Geochemical Journal*, *1*(4), 169-182.

Robert-Baldo, G. L., Morris, M. J., & Byrne, R. H. (1985). Spectrophotometric determination of seawater pH using phenol red. *Analytical Chemistry, 57*(13), 2564-2567.

Sarmiento, J.L., Gruber, N. (2006) *Ocean Biogeochemical Dynamics. Princeton: Princeton University Press.*

Schiebel, R. (2002) Planktonic foraminiferal sedimentation and the marine calcite budget, *Global Biogeochem. Cycles, 16, 1065, doi:10.1029/2001GB001459*.

Schott, J., Oelkers, E. H., Bénézeth, P., Goddéris, Y., & François, L. (2012) Can accurate kinetic laws be created to describe chemical weathering? *Comptes Rendus Geoscience*, *344*(11), 568-585.

Subhas, A. V., Adkins, J. F., Rollins, N. E., Naviaux, J., Erez, J., & Berelson, W. M. (2017) Catalysis and chemical mechanisms of calcite dissolution in seawater. *Proceedings of the National Academy of Sciences, 114(31), 8175-8180.*

Subhas, A. V., Rollins, N. E., Berelson, W. M., Dong, S., Erez, J., & Adkins, J. F. (2015) A novel determination of calcite dissolution kinetics in seawater. *Geochimica et Cosmochimica Acta*, *170*, 51-68.

Sulpis, O., Lix, C., Mucci, A., & Boudreau, B. P. (2017). Calcite dissolution kinetics at the sediment-water interface in natural seawater. *Marine Chemistry, 195, 70-83.*

Takahashi, T. (1975) Carbonate chemistry of seawater and the calcite compensation depth in the oceans: Special publication of the Cushman Foundation, *Foraminiferal Res., 13, 11– 126, 1975.*

Taylor, A. S., Blum, J. D., & Lasaga, A. C. (2000) The dependence of labradorite dissolution and Sr isotope release rates on solution saturation state. *Geochimica et Cosmochimica Acta*, *64*(14), 2389-2400.

Teng, H. H. (2004) Controls by saturation state on etch pit formation during calcite dissolution. *Geochimica et Cosmochimica Acta*, *68*(2), 253-262.

Thunell, R. C., Keir, R. S., & Honjo, S. (1981) Calcite dissolution: An *in situ* study in the Panama Basin. *Science*, *212*(4495), 659-661.

Uppström, L. R. (1974) The boron/chlorinity ratio of deep-sea water from the Pacific Ocean. *Deep. Res. Oceanogr. Abstr. 21, 161–162.*

Van der Wal, P., R. S. Kempers, and M. J. W. Veldhuis (1995) Production and downward flux of organic matter and calcite in a North Sea bloom of the coccolithophore Emiliania huxleyi. *Mar. Ecol. Prog. Ser., 126, 247– 265*.

Walter, L. M., & Morse, J. W. (1985) The dissolution kinetics of shallow marine carbonates in seawater: a laboratory study. *Geochimica et Cosmochimica Acta*, *49*(7), 1503-1513.

White, M. M. et al. (2016) Calcium Carbonate Dissolution Above the Lysocline: Implications of Copepod Grazing on Coccolithophores. *Ocean Sciences Meeting Abstract.*

Xu, J., Fan, C., & Teng, H. H. (2012) Calcite dissolution kinetics in view of Gibbs free energy, dislocation density, and pCO_2. *Chemical geology*, *322*, 11-18.

Xu, M., Hu, X., Knauss, K. G., & Higgins, S. R. (2010). Dissolution kinetics of calcite at 50–70° C: An atomic force microscopic study under near-equilibrium conditions. *Geochimica et Cosmochimica Acta, 74(15), 4285-4297.*

Figure Caption

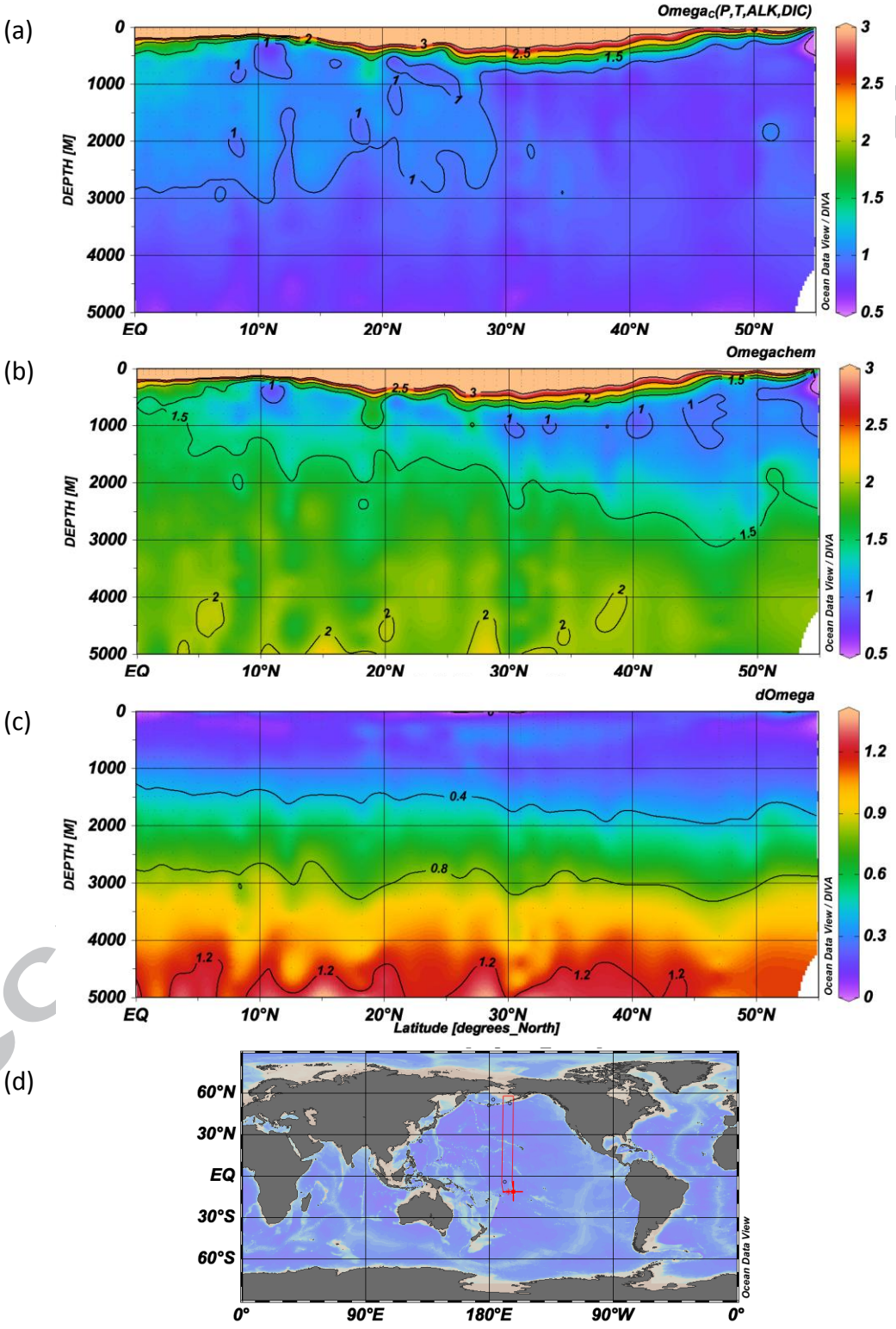

Fig.1 Separation of effect of water chemistry and pressure on $\Omega_{calcite}$ in a Pacific section by Ocean Data View simulation. (a) Ω_{real}: actual Ω. (b) $\Omega_{chemistry}$: Ω calculated by Ocean Data View if there is no effect of pressure on K^*_{sp} (K^*_{sp} after Mucci, 1983), namely Ω affected only by water chemistry (DIC, alkalinity, salinity, temperature). (c) ΔΩ: difference between (b) and (a), Ω affected by pressure; up to 1.2 Ω units at 5000 m depth. (d) Defined section (red box) on map.

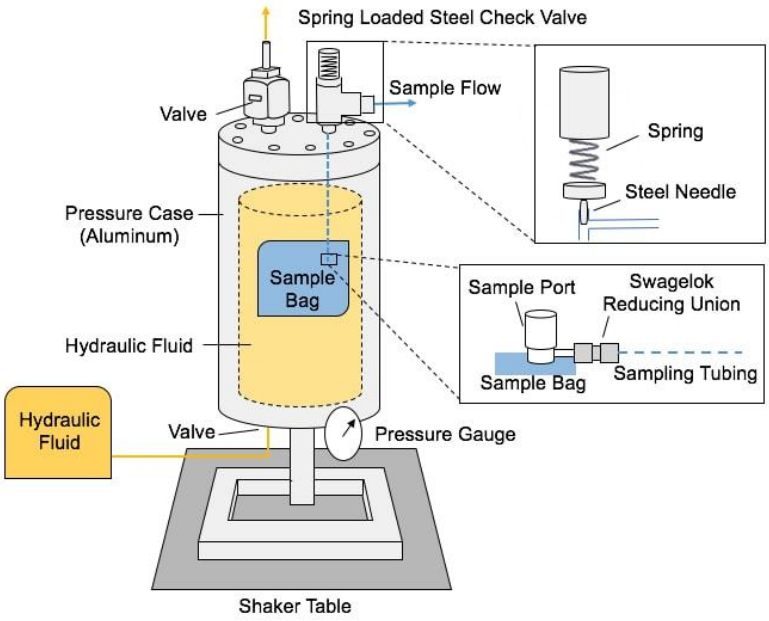

Fig. 2 Pressure Case Diagram

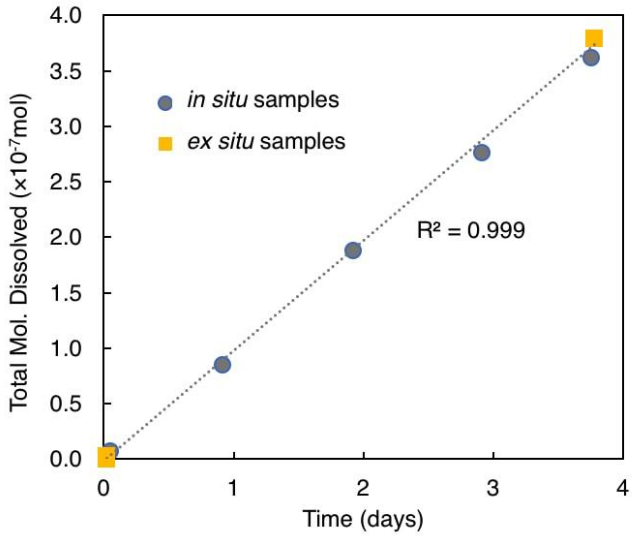

Fig. 3 Moles of labeled carbonate dissolved based on $\delta^{13}C$ measurement from P45 (1050 dbar). Yellow squares are *ex situ* samples (three before experiment, three after experiment); grey circles are *in situ* samples; trend line is fit to all data points. Replicate value uncertainties are less than the size of the data points. Note that only 4×10^{-7} mol calcite was dissolved over 4 days (0.001% of total calcite powder).

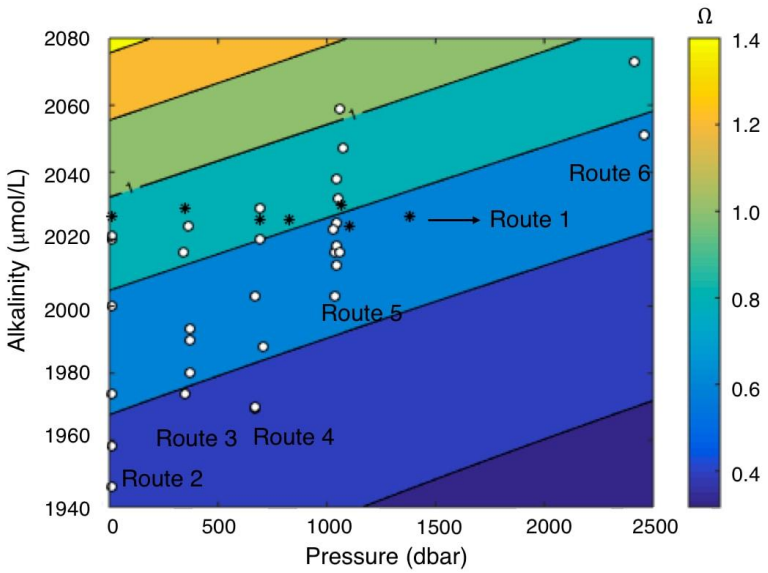

Fig. 4 Ω contour plot as a function of pressure and alkalinity. Six sets of experiments were conducted. Black asterisks were dissolution experiments conducted with the same fill bag seawater, Ω changed by changing pressure (Route 1). White circles were dissolution experiments conducted under five different constant pressures (Route 2 – 10 dbar; Route 3 – 350 dbar; Route 4 – 700 dbar; Route 5 – 1050 dbar; Route 6 – 2500 dbar). Note that this diagram is only a rough demonstration of Ω and experimental parameters, because DIC in this plot has to be set to a fixed value (2030 µmol/kg) while actual DIC for different experiments (different batches of Dickson seawater) vary from 2000 µmol/kg to 2040 µmol/kg.

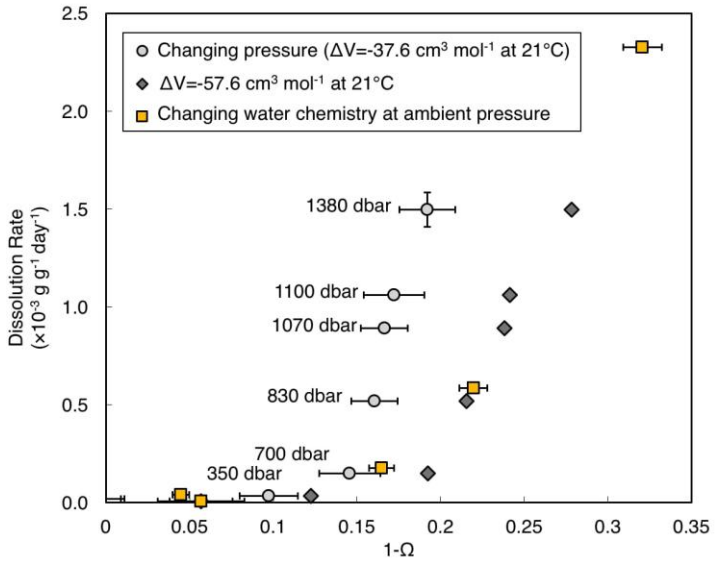

Fig. 5 Dissolution rate vs. undersaturation. Yellow squares: changing water chemistry at atmospheric pressure and 21°C (Route 2 in Fig. 4). Light grey circles: changing pressure with the same fill-bag seawater at 21°C (Route 1 in Fig. 4), ΔV=-37.6 cm^3 mol^{-1} at 21°C (Ingle, 1975). Dark grey diamonds: changing pressure with the same fill-bag seawater, Ω recalculated with ΔV=-57.6 cm^3 mol^{-1} at 21°C (error bars not shown). Pressures at which dissolution experiments were conducted (light grey circles) were 350 dbar, 700 dbar, 830 dbar, 1070 dbar, 1100 dbar, 1380 dbar (marked on the plot). Uncertainties in Ω represent standard deviation of replicates in DIC and alkalinity measurements; uncertainties in dissolution rate represent goodness of fits in Fig. 3.

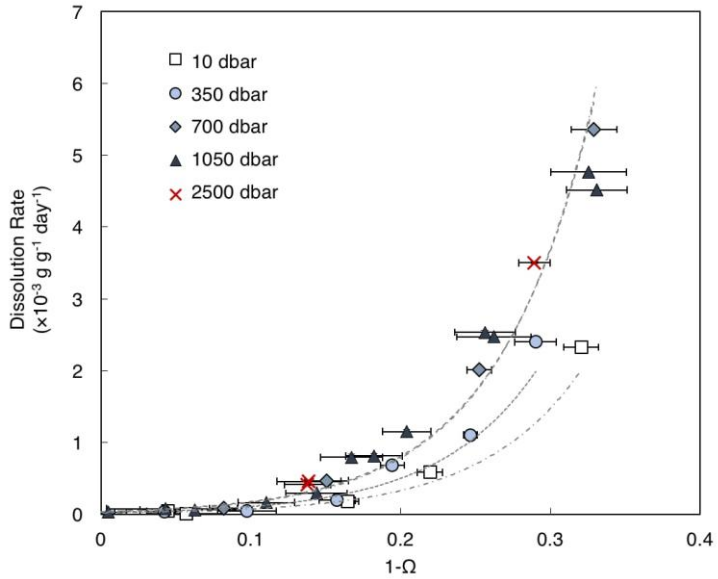

Fig. 6 Dissolution rates versus undersaturation at 5 different pressures (Routes 2-6 in Fig.4). Dashed lines are fits to data points of 10 dbar, 350 dbar, 700 dbar, 1050 dbar. Fits to 700 dbar and 1050 dbar overlap such that these data are fitted to the same curve.

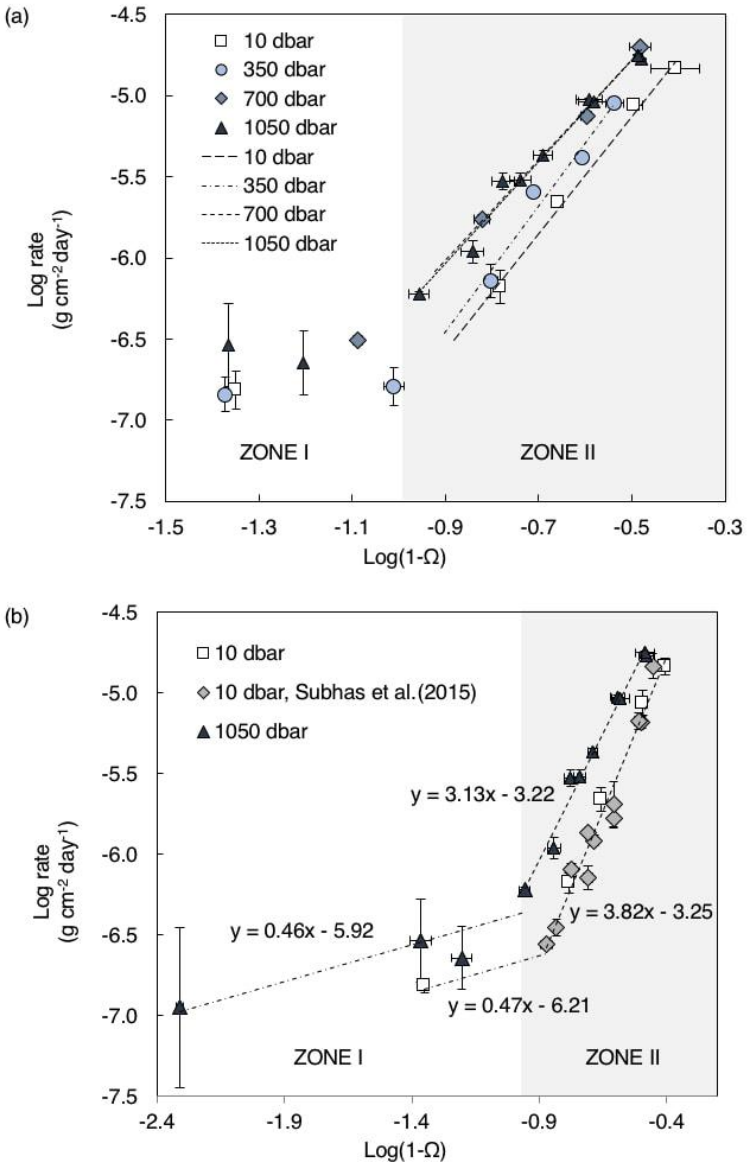

Fig. 7 (a) Log-log plot of geometry-normalized dissolution rate versus undersaturation state at 10, 350, 700, 1050 dbar. Dashed lines are fits to data points in Zone II. For reference, log(1- Ω) from -1.5 to -0.3 is equivalent to Ω = 0.97 to 0.50. (b) Log-log plot of dissolution rate versus undersaturation state. White squares are 10 dbar data from this study; grey diamonds are 10 dbar data from Subhas et al. (2015) using the calcite sample from the same batch, and the same experimental set-ups; black triangles are 1050 dbar from this study. At near-equilibrium conditions, where dissolution rates are very low (Zone I), error bars in log scale plot are large. Irrespective, dissolution rates are clearly off the trend lines in Zone II. Linear regression fits are given.

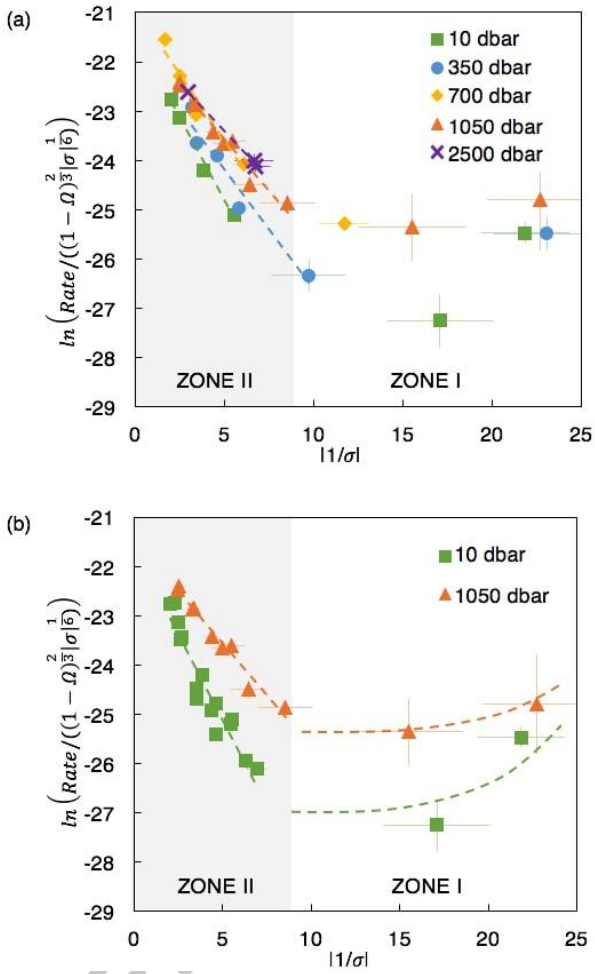

Fig. 8 Dissolution velocity (m/s) versus $|1/\sigma|$ where $|\sigma| = \ln(\Omega)$ (framework proposed by Dove et al. (2005)). Higher $|1/\sigma|$ value means closer to saturation ($\Omega = 1$). Dissolution velocity are off the linear trend lines in Zone I and start to increase as $|1/\sigma|$ increases, indicating a change from step retreat dissolution mechanism (Zone I) to defect-assisted dissolution mechanism (Zone II). Different slopes of different pressure trend lines in Zone II indicate different local interfacial energy barrier α under different pressures (Table 3). (a) Dissolution velocity (m/s) versus $|1/\sigma|$ for 10, 350, 700, 1050, 2500 dbar. (b) Dissolution velocity (m/s) versus $|1/\sigma|$ for 10 dbar (including data from Subhas et al. (2015)) and 1050 dbar only, to show a clearer difference of slopes in Zone II and a clearer change of mechanism at around $|1/\sigma|$=9, equivalent to $\Omega = 0.89$. The trend lines in Zone 1 are schematic fits to the data.

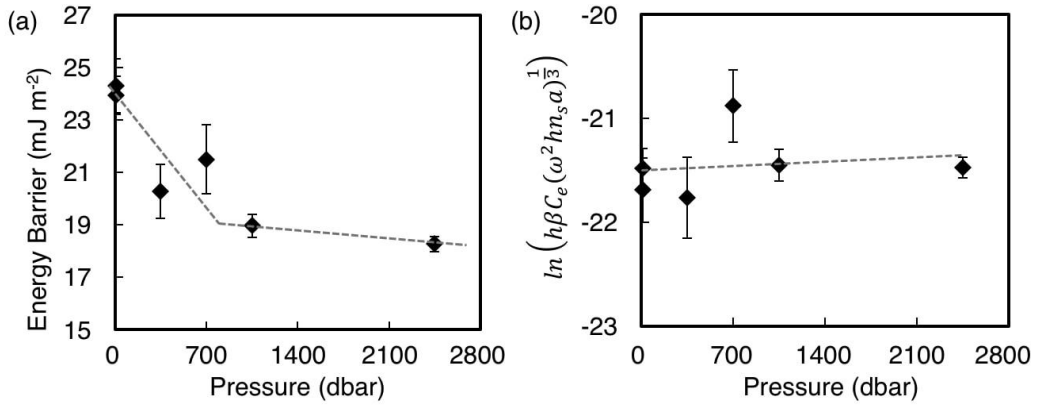

Fig. 9 (a) Surface energy barrier α (calculated from slopes in Fig. 8) versus different pressure. The trend line is a schematic to emphasize the apparent change in slope in α vs. pressure. (b) Change in the intercepts (proportional to kinetic parameters β and/or n_s) versus different pressure for defect-assisted dissolution (Zone II);

Table Caption

Table 1 Coefficients for the effect of pressure on the dissociation constants of acids in seawater.

Acid	$-a_0$	a_1	a_2	$-b_0$	b_1
H_2CO_3	25.50	0.1271	0	3.08	0.0877
HCO_3^-	15.82	-0.0219	0	-1.13	-0.1475
$CaCO_3$ (calc.)	48.76	0.5304	0	11.76	0.3692
$CaCO_3$ (arag.)	35	0.5304	0	11.76	0.3692

Table 2 Apparent partial molal volume changes for calcite dissolution

Substance	T (°C)	ΔV ($cm^3\ mol^{-1}$)	Author
Calcite	25	-34.4	Ingle (1975)
Iceland spar	25	-35.5	Ingle (1975)
Calcite	25	-39.4	Millero and Berner (1969)
Calcite	20	-43.4	Duedall (1972)
Foraminifera	22	-30.7	Pytkowicz and Fowler (1967)
Foraminifera	25	-31.8	Pytkowicz and Fowler (1967)
Calcite	2	-42.3	Ingle (1975)
Calcite	2	-43.8	Sayles (1980)
Oolite	2	-31.8	Ingle (1975)
Oolite	2	-33.1	Hawley and Pytkowicz (1969)

* ΔV values in white boxes are under 20-25°C, temperature comparable to this study (21°C). ΔV values in grey boxes are under 2°C for reference.

Table 3 Fits to Fig. 8 & 9 and calculated local interfacial energy barrier α (mJ/m^2) under different pressure

Pressure (dbar)	Defect-Assisted Dissolution			Note
	Intercept $\ln(\hbar\beta C_e(\omega^2\hbar n_s a)^{\frac{1}{3}})$	Slope $-\frac{\pi\alpha^2\omega\hbar}{3(k_bT)^2}$	Energy Barrier α (mJ m^{-2})	
10	-21.5±0.2	-0.67±0.05	24±1	
10	-21.7±0.3	-0.69±0.07	24±1	*
350	-21.8±0.4	-0.48±0.07	20±1	
700	-20.9±0.4	-0.54±0.09	22±1	
1050	-21.5±0.2	-0.42±0.03	19±1	
2500	-21.5±0.1	-0.39±0.02	18±1	

* Including data from Subhas et al. (2015) (revised).